



## Study of the hydration of CaO powder by gas-solid reaction

Eric Serris, Loïc Favergeon, Michèle Pijolat, Michel Soustelle, Patrice Nortier, Robert Gartner, Thierry Chopin, Ziad Habib

► **To cite this version:**

Eric Serris, Loïc Favergeon, Michèle Pijolat, Michel Soustelle, Patrice Nortier, et al.. Study of the hydration of CaO powder by gas-solid reaction. *Cement and Concrete Research*, Elsevier, 2011, 41 (10), pp.1078-1084. <10.1016/j.cemconres.2011.06.014>. <hal-00613013>

**HAL Id: hal-00613013**

**<https://hal.archives-ouvertes.fr/hal-00613013>**

Submitted on 2 Aug 2011

**HAL** is a multi-disciplinary open access archive for the deposit and dissemination of scientific research documents, whether they are published or not. The documents may come from teaching and research institutions in France or abroad, or from public or private research centers.

L'archive ouverte pluridisciplinaire **HAL**, est destinée au dépôt et à la diffusion de documents scientifiques de niveau recherche, publiés ou non, émanant des établissements d'enseignement et de recherche français ou étrangers, des laboratoires publics ou privés.

1 « Study of the hydration of CaO powder by gas-solid reaction »

2  
3 Serris.E<sup>1\*</sup>, Favergeon.L<sup>1</sup>, Pijolat.M<sup>1</sup>, Soustelle.M<sup>1</sup>, Nortier.P<sup>2</sup>, Gärtner.R.S<sup>3</sup>, Chopin.T<sup>3</sup>, Habib,  
4 Z.<sup>3</sup>

5  
6 <sup>1</sup> Ecole Nationale Supérieure des Mines de Saint-Etienne, centre SPIN, LPMG FRE 3131 CNRS,  
7 158 cours Fauriel 42023 Saint-Etienne, France

8 <sup>2</sup> LGP2, Grenoble INP, 461 rue de la Papeterie, 38402 Saint Martin d'Hères, France

9 <sup>3</sup> Lhoist Recherche et Développement SA, 31 rue de l'industrie, B-1400 Nivelles, Belgium

10  
11 **Abstract:** Hydration of CaO powders by reaction with water vapor has been studied in  
12 isothermal and isobaric conditions. Experimental tests were performed within the temperature  
13 range of 70°C - 420°C and with a water vapor pressure from 5 to 160 hPa by means of a  
14 thermogravimetric device. Two powders, exhibiting slight differences in their physical  
15 properties, were studied. However, for one of the powders and under some temperature and  
16 pressure conditions, the reaction is not complete. The difference of behavior between both CaO  
17 powders was interpreted by considering the effect of the morphological properties on the  
18 mechanism of growth of Ca(OH)<sub>2</sub>.

19  
20 **Keywords:** A kinetics; A hydration; B microstructure; D CaO; anti-Arrhenius

21 **1. INTRODUCTION**

22

23

24 Hydration of calcium oxide (lime) by liquid water is a very well known reaction due to large  
25 domain of applications of hydrated calcium oxide in industry [1, 2]. It is however surprising to  
26 see that only few papers have been published on the “dry” hydration of CaO or the interaction of  
27 water vapor with this oxide [3-6] in comparison with the recent growing interest of studies about  
28 CO<sub>2</sub> interactions on calcium oxides [7-9].

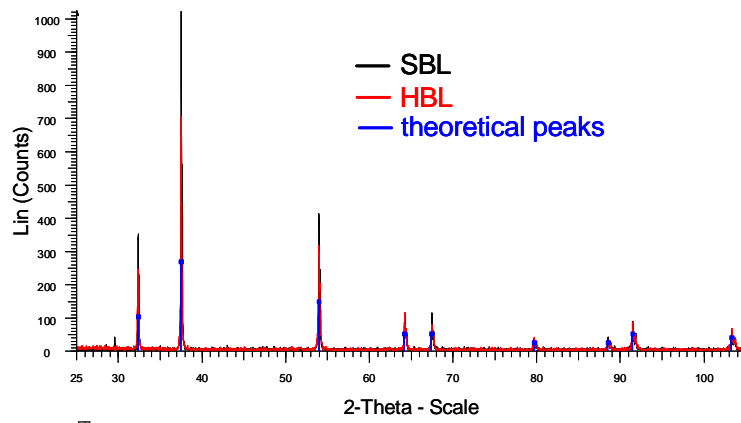
29 D.R.Glason [3] studied the interaction of water vapor with different kinds of lime with specific  
30 surface areas from 1 to 100m<sup>2</sup>.g<sup>-1</sup> and he observed the agglomeration of particles during  
31 hydration at room temperature. A theoretical model for this reaction has been developed [4] with  
32 some experiments on CaO pellets at different water vapor pressure and temperature. They found  
33 that the two most important variables were the water vapor pressure and the calcination  
34 temperature. In some recent works [5-6] on CaO based sorbents, an anti-Arrhenius behavior was  
35 observed and the author linked this phenomenon to the initial content of CaO. They also studied  
36 the CaO hydration and Ca(OH)<sub>2</sub> decomposition over a multitude of cycles with as starting  
37 material crushed and sieved limestone (CaCO<sub>3</sub>). The hydration rate decreased with increasing  
38 number of cycles.

39 The aim of this work is to reach a better knowledge of the mechanism of this reaction, studying  
40 the influence of the water pressure and temperature. Two distinct CaO powders were used under  
41 the same experimental conditions and the differences, observed on the curves giving the  
42 fractional extent of the reaction versus time, are discussed on the bases of the growth mechanism  
43 of the hydroxide and morphology of the two powders.

## 44 **2. MATERIALS AND METHODS**

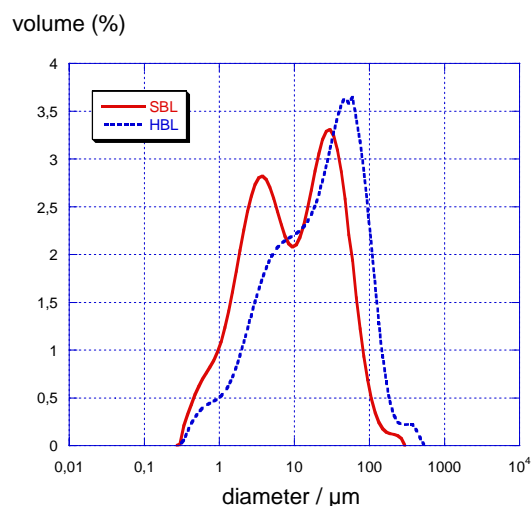
45            **2.1. Materials**

46    The two types of powders used in this work were provided by Lhoist R&D SA. The first one was  
47    called “SBL” (Soft Burnt Lime) and the second one “HBL” (Hard Burnt Lime). The chemical  
48    analysis shows that SBL powder is composed of 94.7% in weight of CaO and HBL powder of  
49    96.4% of CaO. The unburnt part is 2.8 % in SBL instead of 0.7 % in HBL. The other impurities  
50    are in the same proportions in both powders. Then the X-Ray patterns show the standard peaks  
51    for well crystallized CaO (Halite structure) for both the SBL and the HBL sample.  
52



54            **Figure 1 : XRD patterns of both powders**

55    Particle size distributions (PSD) were obtained by means of laser diffraction performed on a  
56    Malvern Mastersizer 2000 and the results are shown in Figure 2. Both distributions are mainly  
57    bimodal. Both products exhibit aggregates of about seventy microns and also small particles of  
58    less than ten microns. The 90% cumulated mass fraction is 94  $\mu\text{m}$  for SBL and 95  $\mu\text{m}$  for HBL.



59

60

**Figure 2 : Particle size distribution of the powders**

61

The specific surface area obtained by measuring nitrogen adsorption isotherms at 77K (BET

62

method) with a micromeritics ASAP 2000 was found to be  $1.42 \pm 0.01 \text{ m}^2 \cdot \text{g}^{-1}$  for HBL sample

63

and  $2.16 \pm 0.01 \text{ m}^2 \cdot \text{g}^{-1}$  for SBL sample. Comparing the equivalent diameter of the individual

64

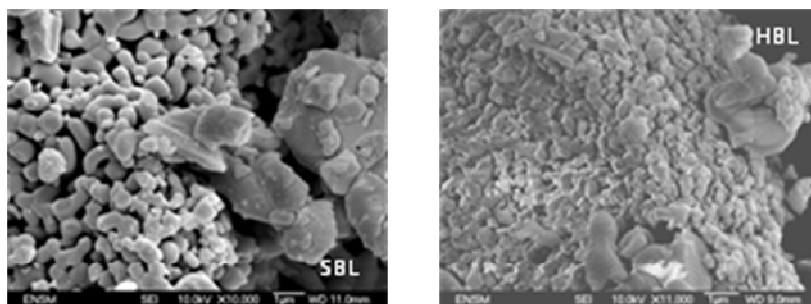
particles obtained from these values to the PSD results indicates that the bigger size peaks of

65

Figure 2 correspond to porous aggregates of smaller particles. This has been confirmed by

66

scanning electron microscopy (Jeol JSM 6500F) as shown by Figure 3.

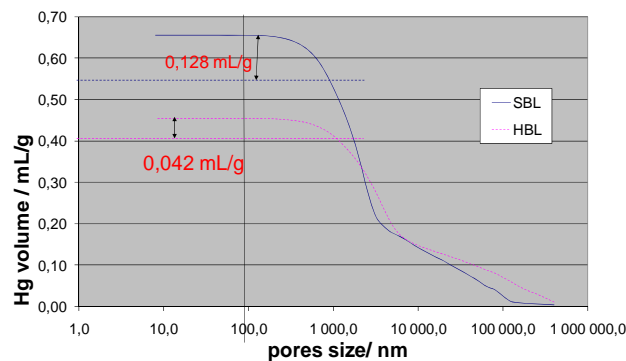


67

68

**Figure 3: Microstructure of the SBL (a) and the HBL (b) CaO aggregates**

69 For SBL the number of small particle seems to be greater than for HBL, as shown by the PSD  
70 curves. Indeed, it is clear from Figure 3 that the internal pores inside the SBL aggregates are  
71 larger than inside HBL ones.



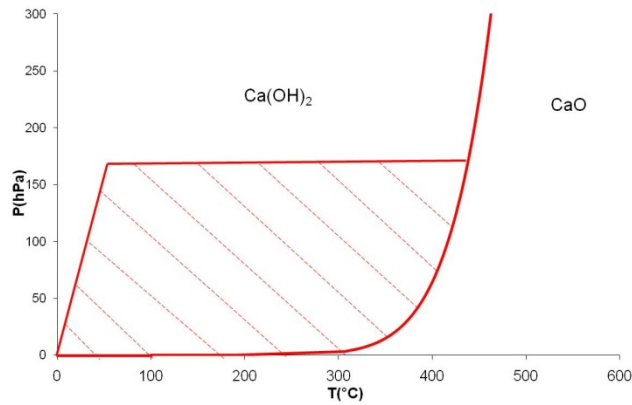
72

73 **Figure 4 : Pore volume distribution as a function of pore diameter for SBL and HBL CaO**  
74 **powders**

75 This has been confirmed by pore volume distributions obtained by mercury intrusion  
76 porosimeter (Micromeritics Autopore IV). Figure 4 shows the cumulative pore volume as a  
77 function of a pore diameter. We can notice both intra-granular and inter-granular voids. If we  
78 consider pores with diameters lower than 1  $\mu\text{m}$ , it is clear that the pore volume inside the SBL  
79 aggregates ( $0.128 \text{ mL.g}^{-1}$ ) is much higher than that inside the HBL aggregates ( $0.042 \text{ mL.g}^{-1}$ ).

## 80 **2.2. Methods**

81 All experiments have been performed at fixed Temperature ( $T$ ) and water vapor partial pressure  
82 ( $P$ ) in a symmetrical thermobalance SETARAM TAG 24 associated with a water vapor  
83 generator Wetsys.

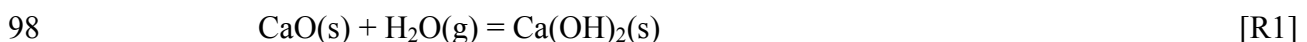


84

85 **Figure 5 : Equilibrium pressure of hydration of calcium oxide and experimental**  
 86 **exploration field**

87 The procedure was the same for all thermogravimetric (TG) experiments. All experiments were  
 88 realized in isobaric and isothermal conditions. The sample temperature was raised up to the  
 89 isothermal step and then the gases (helium and water vapor) were introduced. According to NIST  
 90 data [10] the equilibrium pressure of calcium oxide hydration is represented in Figure 5 by the  
 91 plain curve.

92 With the Wetsys vapor generator, we could achieve water vapor pressures up to 160 hPa in  
 93 helium flux. So our experimental field is included in the hatched area between the equilibrium  
 94 curve and the dotted lines. All the experiments have been carried out far from equilibrium  
 95 conditions - so much so that the corresponding term in the expression of the rate can be left out.  
 96 The TG software gave us mass variation versus time. We transformed this data into fractional  
 97 extent  $\alpha$  of the reaction according to the chemical reaction [R1]:



99 The theoretical mass gain at  $\alpha=1$  should be of +32% of the initial mass of CaO. This initial mass  
 100 is obtained after the experiment with a complete dehydration of Ca(OH)<sub>2</sub>. Thus, we can calculate  
 101 the hydrated part of the initial product.

102 Derivation of the  $\alpha(t)$  curves allows us to calculate the rate of reaction ( $d\alpha/dt$ ), which can be  
103 represented graphically versus  $\alpha$ , to compare the results of experiments carried out in various  
104 temperature and water pressure conditions.

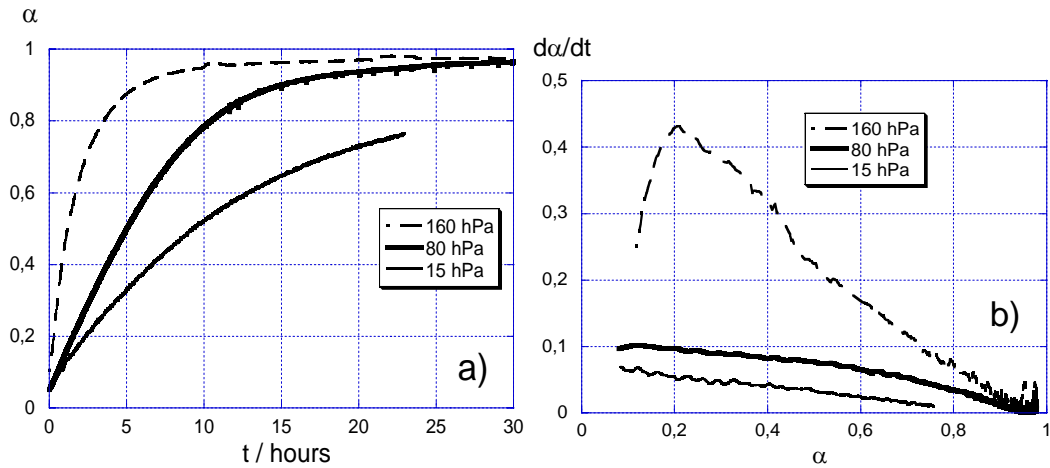
### 105 **3. EXPERIMENTAL RESULTS**

#### 106 ***3.1. Influence of water vapor pressure***

107  
108 The influence of the water vapor pressure on the kinetic curves is illustrated in Figure 6. All  
109 experiments were realized with the SBL powder. The temperature was fixed at 150°C for all  
110 tests.

111 According to the experimental  $\alpha(t)$  curves, the higher the pressure, the faster the reaction (Figure  
112 6a). The maximal fractional extent observed for 80 and 160 hPa reaches mainly 1, which means  
113 that SBL powder can be totally transformed into  $\text{Ca}(\text{OH})_2$ . The rate versus  $\alpha$  curve exhibits a  
114 maximum for the higher pressure experiment. It seems that all the curves present such a  
115 maximum close to the initial time.





116

117 **Figure 6 : influence of water vapor pressure on the hydration of SBL CaO powders at**

118

**150°C :  $\alpha(t)$  (a) and  $d\alpha/dt$  (b)**

119

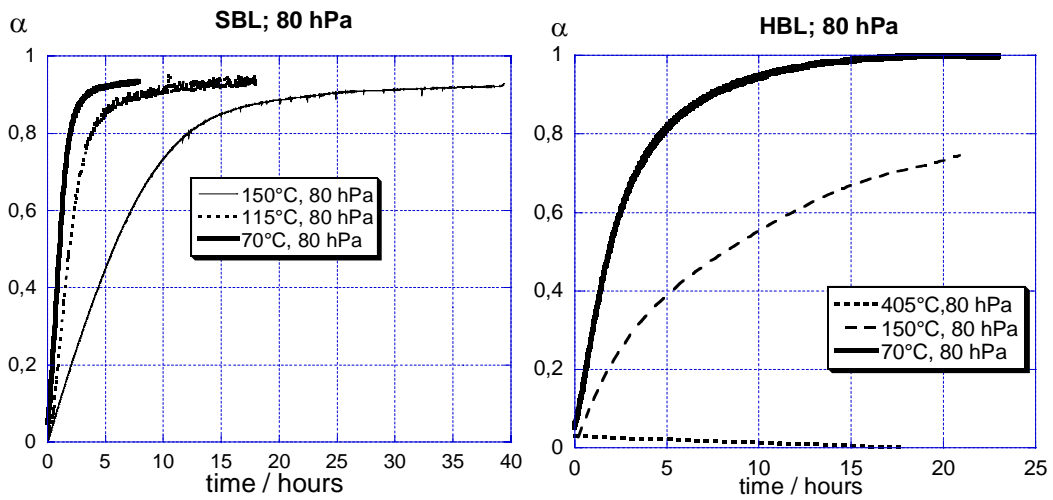
### 3.2. Influence of temperature

120

121 Figure 7 shows  $\alpha(t)$  curves obtained at various temperatures for SBL and HBL samples.

122 It can be seen that for both powders the higher the temperature, the slower the hydration. This  
 123 can be observed from the  $d\alpha/dt(\alpha)$  curves shown in Figure 8 for SBL CaO powder. Such a  
 124 behavior is quite unusual.

125 We could also note that the maximum of the curves moves from  $\alpha=0.05$  to nearly 0.4 when  
 126 temperature increased.



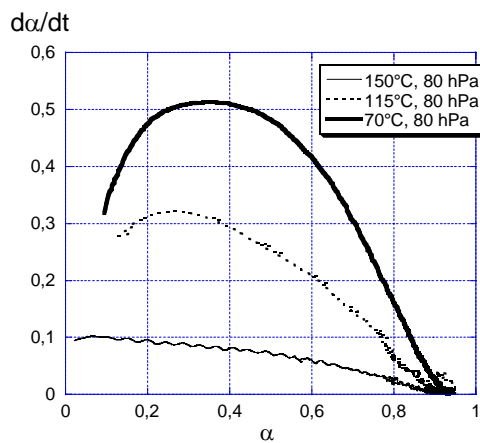
127

128

**Figure 7: Influence of temperature on hydration of SBL and HBL CaO powders with a water vapor pressure equal to 80 hPa**

129

130



131

132

133

134

135

**Figure 8 : Influence of the temperature on the kinetic rate of hydration of SBL CaO powder with a water vapor pressure of 80 hPa**

136

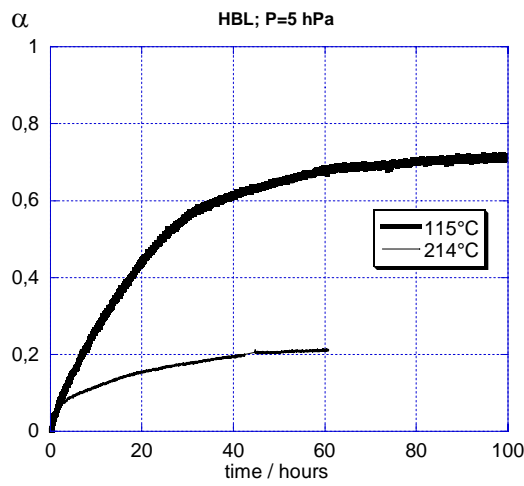
137

138

**3.3. Maximal extent of reaction: “blocking effect”**

139

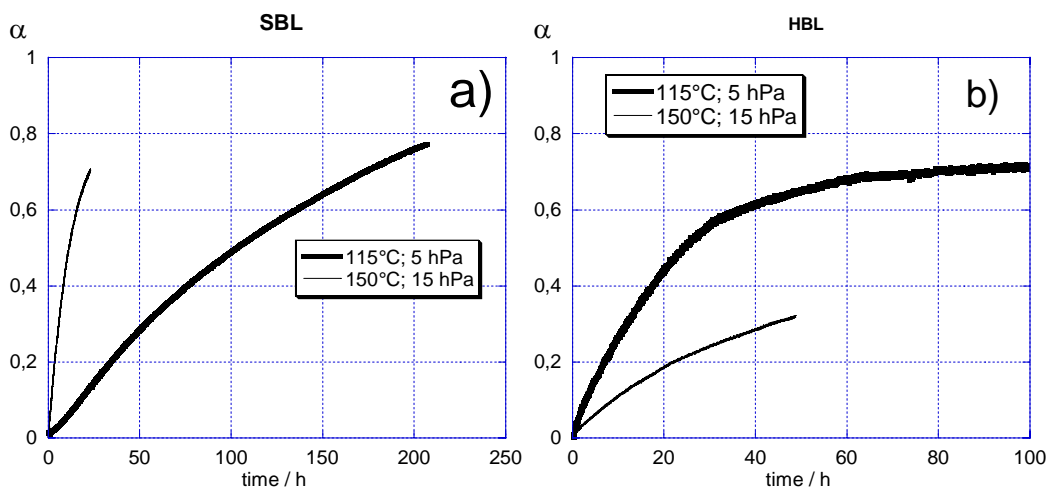
140 For HBL CaO powder and in some experimental conditions of dry hydration, the reaction was  
 141 not complete and stopped at a fractional extent lower than 1. During the reaction something  
 142 happen (for example a diffusion through the hydroxide layer became extremely slow) and the  
 143 reaction rate is so slow that we can consider that the reaction is blocked. We will call this  
 144 phenomenon the “blocking effect” in the following. Two curves of the fractional extent versus  
 145 time are represented in figure 9 for two different temperatures with 5 hPa of water pressure.



146

147 **Figure 9: blocking effect for HBL powder**

148 The maximal value reached by the fractional extend depends for each powder on the operating  
 149 conditions (temperature and water vapor pressure). Only HBL CaO powder exhibited such a  
 150 behavior, as illustrated in Figure 10. Same experimental conditions were use (115°C, 5 hPa and  
 151 150 °C, 15 hPa) for both HBL and SBL experiments.



152

153 **Figure 10 : Fractional conversion versus time incross over experiments on (a) SBL and (b)**  
154 **HBL CaO powders**

155 For HBL the blocking effect is clearly observed at 115°C and 5 hPa since a plateau is reached for  
156  $\alpha$  equal to 0.7. In the other experiment (150°C and 15 hPa), it can be foreseen that the fractional  
157 extent will not exceed 0.5. For SBL however, both reactions were not finished but the fractional  
158 conversion has reached values above 0.75 and does not seem to stop increasing well below 1.

159 **4. DISCUSSION, MECHANISM OF THE REACTION**

160 **4.1. Kinetic laws**

161 If we consider the hydration of SBL samples, the rate curves such as those in Figure 6b or Figure  
162 8, exhibit a maximum, which suggests that the reaction involves simultaneous nucleation and  
163 growth processes of the new phase ( $\text{Ca(OH)}_2$  in our case). In general [11], kinetic modeling of  
164 these reactions are done using a general expression of the reaction rate in the form  $d\alpha/dt = A \exp(-$   
165  $E/RT) \cdot f(\alpha)$  where  $A$  is a pre-exponential factor,  $E$  a temperature coefficient called apparent  
166 activation energy in the litterature,  $R$  the perfect gas constant,  $T$  the temperature and  $f(\alpha)$  a  
167 function of the fractional conversion  $\alpha$  (in the case of sigmoid  $\alpha(t)$  curves, authors often use the  
168 Avrami laws  $A_n$  or the Prout-Tompkins law B1). Nevertheless, Avrami laws and Prout-  
169 Tompkins law are not usable in the case of solid-gas reactions; and moreover the use of  
170 temperature dependence following an Arrhenius behavior should be done with care as explained  
171 in [12]. We use a more general method based on surface nucleation followed by nuclei growth  
172 [13]. This means that nuclei of hydroxide are formed onto the surface of the initial oxide grains

173 with a frequency  $\gamma$ , called the areic frequency of nucleation and expressed in number of nuclei.m<sup>-2</sup>.s<sup>-1</sup>. The nuclei thus formed then grow with a rate  $\phi$  called the areic reactivity of growth and  
174 <sup>2</sup>.s<sup>-1</sup>. The nuclei thus formed then grow with a rate  $\phi$  called the areic reactivity of growth and  
175 expressed in mol.m<sup>-2</sup>.s<sup>-1</sup>. The most common laws used for such a behavior are those of either  
176 Mampel's [14-15] (uniform surface nucleation, isotropic growth, inward development and  
177 internal rate-determining step of growth) or of the different mechanisms with uniform nucleation  
178 and anisotropic growth as Jacobs and Tompkins' model for example [16-17]. Such models are  
179 explained and detailed in reference [18].

180  
181 In this text, we will only consider a general form,  $d\alpha/dt = \phi(P, T, \dots) \cdot f(t)$  [19] if it is supposed that  
182 the growth rate is controlled by an elementary step.  $\phi(T, P, \dots)$  will be expressed by the  
183 theoretical expression deduced from the mechanism of growth and this expression will help us to  
184 interpret experimental behavior (influence of temperature and partial pressure).

#### 185 ***4.2. Proposal of a mechanism for growth and anti-Arrhenius behavior***

186  
187 For the growth of the calcium hydroxide layer, we refer to a traditional mechanism of solid-gas  
188 reaction taking into account both internal (between calcium hydroxide and calcium oxide) and  
189 external (between calcium hydroxide and water vapor) interfaces with diffusion of species  
190 through the hydroxide layer, with the specificity of the calcium hydroxide, which is insulating,  
191 and of water molecules which form easily hydrogen bonds while being likely to dissociate).

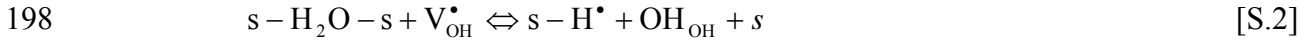
192 The various steps involved in the mechanism are detailed below:

193 At the external interface:

- 194 • The adsorption of water molecules with hydrogen bonds on two sites of adsorption  
195 (noted 's'):



197 • The formation of an hydroxide group from an hydroxide vacancy:



199 • The reaction between hydrogen and an oxygen ion in hydroxide position:



201 In the hydroxide layer:

202 • The diffusion of the hydroxide vacancy and of the oxygen ion from the internal  
203 interface toward the external interface

204 At the internal interface:

205 • The creation of the hydroxide vacancy and the oxygen ion in hydroxide position:



207 A linear combination of steps [S.1], [S.2], [S.3] and [S.4] leads to the overall reaction:



209 The mechanism is solved by using the rate determining step method assuming that step [S.2] is  
210 the rate determining one [20]. We obtain for the areic reactivity of growth:

211  $\phi = \phi_{[2]} = k_2 [s - \text{H}_2\text{O} - s] \cdot [\text{V}_{\text{OH}}^\bullet]$  (E1)

212 We write that all the steps  $i$ , apart from [S.2], are at equilibrium with the corresponding  
213 equilibrium constant  $K_i$  and the electric neutrality:

214  $[s - \text{H}^\bullet] + [\text{V}_{\text{OH}}^\bullet] = [\text{O}'_{\text{OH}}]$  (E2)

215 Assuming a low coverage of adsorption sites, that is:  $[s - \text{H}_2\text{O} - s] \ll 1$  and  $[s - \text{H}^\bullet] \ll 1$ , the areic  
216 reactivity of growth becomes :

217 
$$\phi = k_2 K_1 K_4 P_{H_2O} \sqrt{\frac{K_3}{1 + K_3 K_4}} \quad (E3)$$

218 According to this solution the areic reactivity of growth should not obey the Arrhenius law with  
 219 temperature, which means that the temperature coefficient  $\Gamma$  does not have the meaning of an  
 220 activation energy unless the condition  $K_3 K_4 \ll 1$  is fulfilled. In this last case, the solution  
 221 becomes:

222 
$$\phi = k_2 K_1 K_4 \sqrt{K_3} P_{H_2O} \quad (E4)$$

223 In this case, we can consider the temperature coefficient as an apparent activation energy  
 224 connected to the activation energy  $E_2$  of the rate determining step (formation of a hydroxide  
 225 group from a hydroxide vacancy) and with the enthalpy  $\Delta H_i$  of the various steps  $i$  constantly at  
 226 equilibrium:

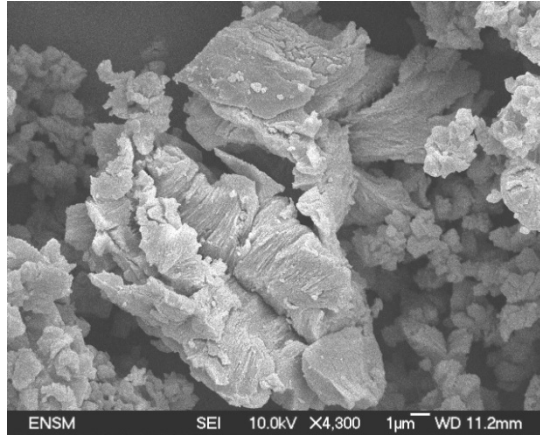
227 
$$\Gamma = E_a = E_2 + \Delta H_1 + \frac{\Delta H_3}{2} + \Delta H_4 \quad (E5)$$

228 One can note, that there is indeed every chance that the preceding linear combination of the  
 229 enthalpies is strongly negative, knowing that only the enthalpy of the rate determining step does  
 230 not appear in the sum and that the total enthalpy of the reaction is strongly negative. Thus  
 231 negative apparent activation energy is only the translation of strongly exothermic steps preceding  
 232 the rate determining one. This property is known as an anti-Arrhenius behavior.

233 **4.3. The Blocking effect**

234 In order to understand the origin of the blocking affect, the sample obtained at the end of the TG  
 235 experiments were observed by SEM.

236 First, let's see the pictures of hydrated grains in an experiment with no blocking effect. Figure 11  
237 shows hydrated SBL after experiment at 160°C and 160 hPa of water vapour pressure (no  
238 blocking effect).

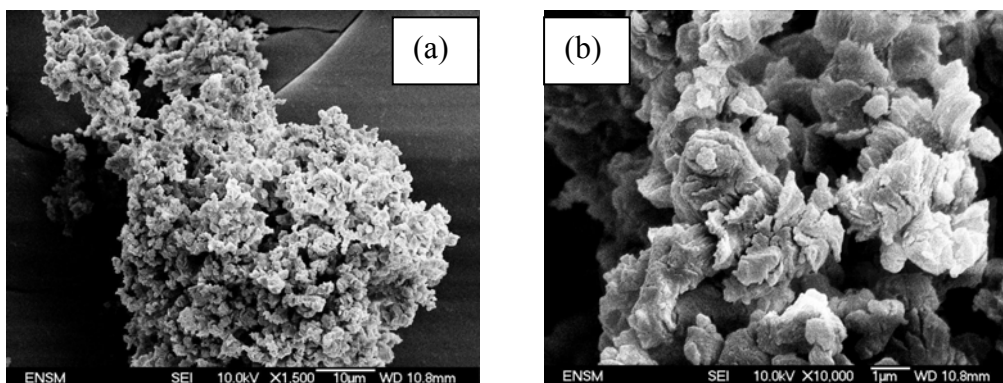


239  
240  
241  
242  
243

244 **Figure 11 : SEM picture of hydrated SBL 115°C, 5 hPa (No blocking effect)**

245 All the grains in the initial aggregate were transformed into  $\text{Ca}(\text{OH})_2$  leading to an arrangement  
246 of grains with a gypsum flower like shape. A lamellar structure can be noticed with thin flakes of  
247 less than 50 nm. This microstructure is in agreement with the hexagonal crystalline structure of  
248 calcium dihydroxide. From observations of different hydrated SBL samples, aggregates in Figure  
249 11 as well as aggregates larger than 50 µm could be observed (cf Figure 12). They are all  
250 composed of assemblies of the same gypsum flower pattern.

251  
252  
253  
254  
255  
256

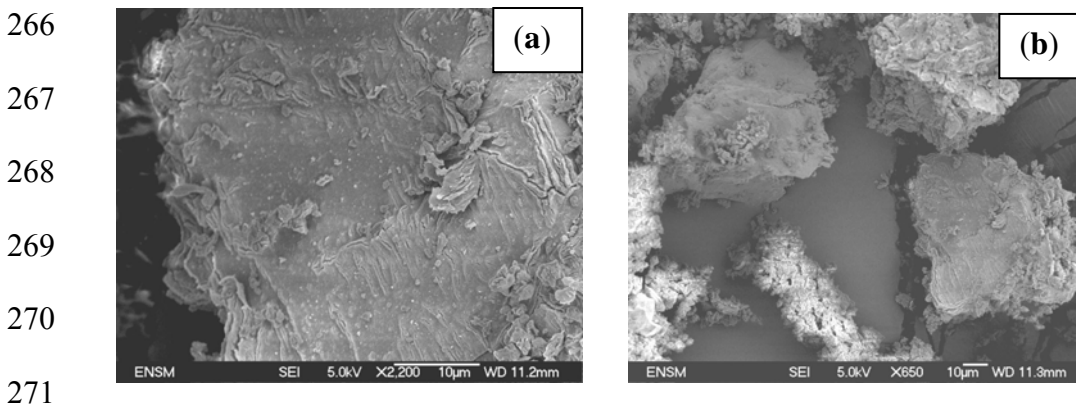




257 **Figure 12 : SEM picture of hydrated SBL 160°C, 80 hPa (No blocking effect) : a) X 1500;**  
258 **b) X 10 000**

259 We can conclude from these observations that even if the transformation strongly modifies the  
260 microstructure of the initial particles, the global structure of the initial aggregates is not  
261 destroyed and they are still porous.

262 Figure 13 shows the morphology of the aggregates (13 b) and the surface of the aggregates (13 a)  
263 in the case of a HBL sample hydrated at 115°C and 5hPa of water vapor pressure. For this  
264 sample, a blocking effect was observed with a value of 0.7 for the maximal fractional extent (cf  
265 Figure 10b).



272 **Figure 13 : SEM picture of hydrated HBL 115°C, 5 hPa (blocking effect)**

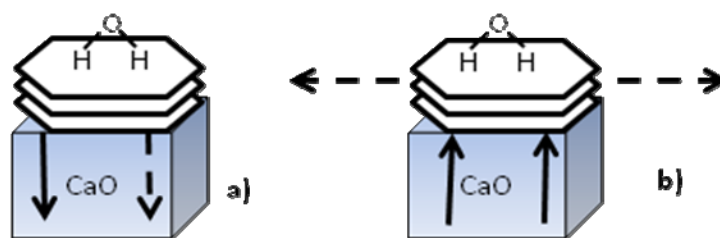
273 Aggregates look here very dense which is very different to the gypsum flower microstructure  
274 observed for the samples without blocking effect. It is not possible to distinguish individual  
275 grains like in the initial aggregates (cf Figure 3b). Furthermore, some faces of the aggregates  
276 look very smooth suggesting that a continuous layer of  $\text{Ca(OH)}_2$  had spread out without pore  
277 formation, only few cracks were formed on these surfaces. On the other faces, however, the  
278 aggregates take more or less the lamellar microstructure previously observed with HBL, with  
279 some porosity.

280 Considering the results obtained in the cross experiment (cf Figure 10), the origin of the blocking  
281 effect may be attributed to the differences in the physical characteristics of both SBL and HBL  
282 CaO powders.

283 SEM observations reveal strong differences between SBL and HBL in the powder morphology  
284 after hydration: continuous superimposed layers for HBL with a global size slightly larger than  
285 the initial aggregates compared to individual grains transformed and gypsum flower pattern in  
286 the aggregates for SBL.

287 From these results we can imagine that the growth of  $\text{Ca}(\text{OH})_2$  may proceed according to two  
288 possible mechanisms. Indeed, calcium dihydroxide crystallizes in hexagonal structure (space  
289 group  $P3m1$ ), which presents a strong anisotropy. So two directions of growth may be  
290 considered: either perpendicular or parallel to the hexagonal planes of the  $\text{Ca}(\text{OH})_2$  structure.

291 Figure 14 illustrates schematically the differences in both possible mechanisms.



292

293 **Figure 14 : Schemes of perpendicular (a) and parallel (b) growth processes. Bold and**  
294 **dashed arrows indicates the direction of diffusing species and of development of  $\text{Ca}(\text{OH})_2$ ,**  
295 **respectively**

296 The so-called perpendicular growth proceeds quite usual in gas-solid reactions: according to the  
297 mechanism described above and the inward advance of the internal interface. In the parallel  
298 mechanism, after the adsorption, the diffusion of calcium and oxygen ions may proceed from the

299 internal interface by the side of the hexagonal planes of  $\text{Ca(OH)}_2$ , thus leading to their possible  
300 extension by reacting with hydroxyls and proton ions present at the surface. This second way of  
301  $\text{Ca(OH)}_2$  growth better explains the gypsum flower microstructure observed by SEM in the  
302 hydrated samples. Thus the parallel mechanism seems to be predominant in both kinds of  
303 powders. However, the perpendicular one may occur too, at least in the firsts moments of the  
304 reaction, and as long as the thickness of  $\text{Ca(OH)}_2$  layer reminds low. In such anisotropic crystals,  
305 the diffusion in the direction perpendicular to the layers is generally slow compared to surface  
306 diffusion, especially at the temperatures investigated in this study (lower than  $420^\circ\text{C}$ ). In the case  
307 of SBL powder, where numerous open pores exist inside the aggregates, the reaction takes place  
308 in each particle separately, without interaction with the neighboring particles. Thus the water  
309 vapor may easily circulate inside the porosity, which is in favor of a total conversion of  $\text{CaO}$  into  
310  $\text{Ca(OH)}_2$ . On the other hand, since the HBL powder is composed of very compact aggregates,  
311 the parallel growth leads to much more continuous layers of  $\text{Ca(OH)}_2$ , which tend to envelop  
312 very large areas of the aggregates. As a consequence, the access of the reacting gas inside the  
313 aggregates is strongly reduced, and it results in an incomplete transformation, the perpendicular  
314 growth being too sluggish in the temperature range investigated (up to  $420^\circ\text{C}$ ).

## 315 **5. CONCLUSIONS**

316  $\text{CaO}$  hydration by water vapor has been investigated using thermogravimetry at constant  
317 temperature and water partial pressure. The curves of the fractional extent versus time obtained  
318 for two distinct  $\text{CaO}$  powders revealed several interesting features:

- 319 – the influence of water vapor pressure enhanced the kinetics of reaction with a linear  
320 dependence of the pressure on the rate;

321 – an anti-Arrhenius behavior was observed for the temperature dependence, due to  
322 extremely exothermic reaction combined with a rate determining step leading to an expression of  
323 the rate including all the steps;

324 – a “blocking effect” was also observed for only one of the powders (less inter aggregate  
325 porosity) with “in fine” packed aggregates attributed to the growth of  $\text{Ca(OH)}_2$  continuous layers  
326 around the aggregates.

## 327 REFERENCES

- 328  
329 [1] H. Shi, Y. Zhao, W. Li, *Cem. Concr. Res.*, 32(5) (2002) 789-793.
- 330 [2] J.-M. Commandré, S. Salvadora and A. Nzihoua, *Chemical Engineering Research and*  
331 *Design*, 85(4) (2007) 473-480.
- 332 [3] D.R. Glasson, *J.appl.Chem.*, 8 (1958) 798-803.
- 333 [4] A. Maciel Camacho, H.R. Hernandez, A.W.D Hills et al, *Isij International*, 37(5) (1997) 468-  
334 476.
- 335 [5] S.Lin, Y.Wang, Y.Suzuki, *Energy & Fuels*, 23(2009) 2855-2861.
- 336 [6] Y. Wang, S. Lin, Y. Suzuki, *Effect of CaO*, *Fuel Process. Technol.* 89 (2008) 220-226.
- 337 [7] P. De Silva, L. Bucea, D.R. Moorehead, V. Sirivatnanon, *Cem. Concr. Comp.*, 28 (2006)  
338 613-620.
- 339 [8] Yi, KB; Ko, CH; Park, JH, et al., *Catalysis Today*, 146(1-2), (2009), 241-247.
- 340 [9] Manovic, V; Charland, JP; Blamey, J, et al., *Fuel*, 88(10), (2009) 1893-1900.
- 341 [10] Chase. M.W., Jr., *NIST-JANAF Thermochemical Tables, Fourth Edition*, *J. Phys. Chem. Ref.*  
342 *Data*, Monograph 9(1998) 1-1951.
- 343 [11] A.K. Galwey, M.E. Brown, *Thermal decomposition of ionic solids*, Elsevier, 1999.

- 344 [12] M.Pijolat, L.Favergeon, M.Soustelle, *Thermochimica acta* (2011) (submitted).
- 345 [13] M.Soustelle “Handbook of heterogeneous kinetics” edited by ISTE - Wiley, London (2010)
- 346 [14] K. L. Mampel, *Z. Phys. Chem., Abt. A*, 187(1940), 235–249.
- 347 [15] W. A. Johnson and R. F. Mehl, *Trans. Amer. Inst. Mining Met. Eng.*, 135 (1939), 416–442.
- 348 [16] P. W. M. Jacobs and F. C. Tompkins, in *Chemistry of the Solid State*, ed. W. E. Gardner,
- 349 Butterworths Scientific Publications, London, 1955, p. 203.
- 350 [17] P. W. M. Jacobs, *J. Phys. Chem. B*, 101 (1997) , 10086–10093.
- 351 [18] M.Soustelle “Handbook of heterogeneous kinetics” edited by ISTE - Wiley, London (2010)
- 352 P. 351-370.
- 353 [19] M.Pijolat, M.Soustelle “Experimental tests to validate the rate-limiting step assumption
- 354 used in the kinetic analysis of solid-state reactions” *Thermochimica acta* , 478 (2008), 34-40
- 355 [20] M.Soustelle “Handbook of heterogeneous kinetics” edited by ISTE - Wiley, London (2010)
- 356 P. 220-233.